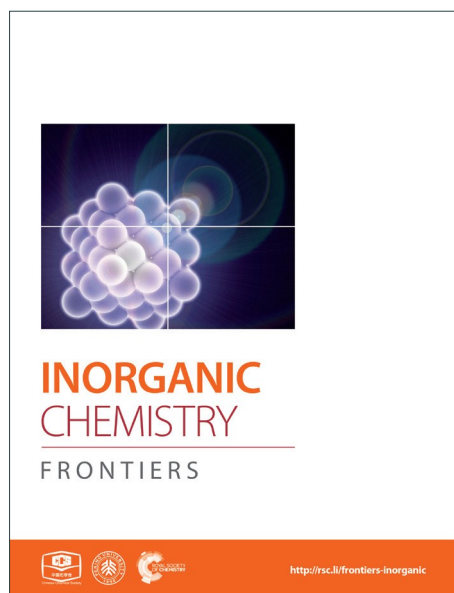
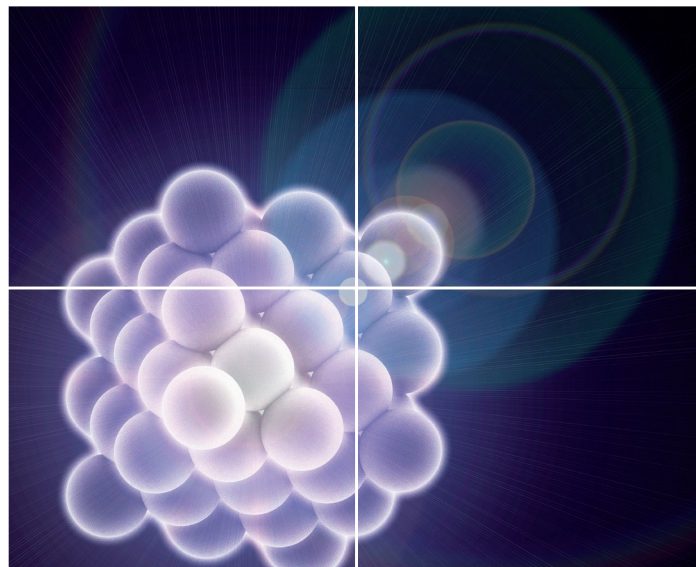


INORGANIC CHEMISTRY

FRONTIERS

Accepted Manuscript



This is an *Accepted Manuscript*, which has been through the Royal Society of Chemistry peer review process and has been accepted for publication.

Accepted Manuscripts are published online shortly after acceptance, before technical editing, formatting and proof reading. Using this free service, authors can make their results available to the community, in citable form, before we publish the edited article. We will replace this *Accepted Manuscript* with the edited and formatted *Advance Article* as soon as it is available.

You can find more information about *Accepted Manuscripts* in the [Information for Authors](#).

Please note that technical editing may introduce minor changes to the text and/or graphics, which may alter content. The journal's standard [Terms & Conditions](#) and the [Ethical guidelines](#) still apply. In no event shall the Royal Society of Chemistry be held responsible for any errors or omissions in this *Accepted Manuscript* or any consequences arising from the use of any information it contains.



Journal Name

ARTICLE

Enhanced electromechanical performance in metal-MgO-ZnO tunneling diodes due to the insulator layers

Yousong Gu^{a,b,†}, Xuhui Yang^{a,†}, Yilin Guan^a, Max A. Migliorato^{a,c}, and Yue Zhang^{a,b,*}

Received 00th January 20xx,
Accepted 00th January 20xx

DOI: 10.1039/x0xx00000x

www.rsc.org/

The enhanced electromechanical performance of metal-insulator-semiconductor tunneling diodes (MISTDs) based on ZnO nanostructures is investigated through modeling in the framework of the Schrödinger equation with the effective-mass approximation. It is found that the performance of ZnO based diodes is greatly improved by inserting an MgO layer which allows the inhibition of screening effect. The piezoelectric response of MISTDs is much higher than that of metal-semiconductor-metal Schottky diodes MSMSDs. The current of the MISTDs is almost zero at -2% compressive strain and increases to a much higher value (~ 600nA) than that of the MSMSDs (~ 400 nA) at +2% tensile strain. The enhancement mechanism of MISTDs is investigated by examining the electron density, electric field, electrostatic potential and conduction band edge of the device. The results found that the origin of the enhanced electromechanical performance is due to the inhibition of screening effects by the insulating MgO layer which leads to a highly strain sensitive energy barrier in the ZnO layer and an extra energy barrier in the MgO layer with a strain modulated height.

1. Introduction

Schottky diodes are important electronic components for the use of nanodevices in optoelectronic and photoelectric applications. Our recent study shows that the insertion of an ultra-thin insulator layer will improve the electric performance of metal-insulator-semiconductor tunnelling diodes (MISTDs) as compared to other conventional Schottky diodes¹. At the same time, piezoelectric potential is created due to strained induced polarization in non-centre symmetric crystals, such as ZnO and GaN. Recently, many studies showed that piezoelectric effect can be employed to modulate the performance of devices based on wurtzite materials³⁻⁶. It has been reported that piezoelectric effects can be used to enhance the performance of electronic and optoelectronic devices based on ZnO nanostructures^{7,8}.

By the combination of piezoelectric and semiconducting properties, piezoelectric semiconductors have been used in many applications, such as strain sensor^{9,10}, nanogenerators^{11,12}, piezoelectric FETs¹³, piezo-phototronic devices^{14, 15}. Recent reports, however, point out that full exploitation of the piezoelectric effect can be hampered by the presence of screening effects and resulting interface energy barrier^{4,12, 16-18}.

Many studies have reported strategies on how to enhance the piezoelectric effect of nano devices, such as controlling both the carrier density in piezoelectric semiconductors and the interfacial energy^{7, 17, 19-22}. For example, Li dopants and insertion of an MoO₃ interlayer between the ZnO/top electrode could remarkably improve sound-driven piezoelectric energy nanogenerator¹⁹. Photo response performance and piezoelectric effect of ZnO based self-powered photodetector are enhanced also by inserting an Al₂O₃ layer²⁰. Thin PMMA spin-coating was used to tailor the piezoelectric potential in piezoelectric nanogenerator^{17,21}.

ZnO is a semiconductor with a direct and wide energy band gap of 3.4 eV, environmentally friendly, chemically stable and of easy synthesis. It hence find wide applications in many fields. ZnO is also a typical piezoelectric materials and can be used in piezoelectric devices²³⁻²⁵, which makes it widely used for applications such as strain sensors²⁶⁻²⁹, nanogenerators³⁰, UV detectors³¹⁻³³, light emitting diodes LEDs³⁴ and laser diodes (LDs)^{35,36}.

We reported in our recent work that the piezoelectric effect in ZnO based nanodevices can be modulated by other factors, such as carrier concentrations³⁷. Furthermore, the piezoelectric properties itself are dependent on the structures of the nanomaterials used³⁸. Performance enhancement were reported for ZnO nanodevices by inserting a thin MgO layer. Au-MgO-ZnO (AMZ) ultraviolet (UV) photodetectors were fabricated by an inserting ultrathin insulating MgO layer, which enhanced their sensitivity due to a reduction of dark current³⁹. Meanwhile, strain modulation was also used to enhance the sensitivities of AMZ UV photodetectors. It presents a prospective approach to engineer the performance of UV photodetectors. By introducing an insulating MgO (*i*-MgO) nanolayer⁴⁰, the performance of a ZnO-MgO-metal

^a School of Materials Science and Engineering, University of Science and Technology Beijing, Beijing 100083, China.

^b Beijing Municipal Key Laboratory of New Energy Materials and Technologies, Beijing 100083, China.

^c School of Electrical and Electronic Engineering, University of Manchester, Manchester M13 9PL, UK

[†] These authors contributed equally to this work.

* Address correspondence to yuezhang@ustb.edu.cn

Electronic Supplementary Information (ESI) available:

strain sensor is significantly improved with an “on/off” current ratio up to 10^5 and a sensitivity of $7.1 \times 10^4 \text{ gf}^{-1}$. The enhancement mechanism is attributed to the combination of piezoelectric effect of ZnO nanoarrays and electron-tunneling modulation of MgO layer, due to the control of the reversible potential barrier height by piezoelectric potential.

In this work, we report our investigation of the enhanced electromechanical performance of an MISTD based on ZnO nanostructures and compare with that of a conventional metal–semiconductor–metal Schottky diode (MSMSD). The coupled Schrödinger–Poisson and current continuity equations for electrons and holes are solved via an effective-mass approximation (EMA), using the Nextnano software⁴¹. The results obtained with our 1D model are valid for thin films, but can be converted and applied to diodes based on ZnO nanowires with a diameter of 100 nm, for comparison with experimental results. The enhancement mechanism of MISTDs were investigated by analysing current–voltage characteristics, the distributions of electron density, electric fields and conduction band edge.

2. Results and discussion

2.1 Enhanced piezoelectric response in MISTD

The current–voltage curves of a MSMSD and a MISTD with 1nm thick MgO layer were calculated under a series of uniaxial strains in the range from -2% to 2%, and the results are shown in Fig.1. Due to the limitation of the nextnano³ package, calculations collapse frequently at high bias voltage and we are can only get reliable results up to 1.0 V bias voltage. For the sake of comparison with experimental results, the calculated current densities are converted into currents of nanowires with a diameter of 100 nm. The magnitude of current of the MSMSD (i.e. without MgO layer) is comparable to the results simulated by a FEM module as implemented in COMSOL Multiphysics package⁴². It shows that our simulation method can yield to accurate results.

In the case of MSMSDs, the currents are quite small at low bias voltage and increase almost linearly at high bias voltage beyond a certain turn-on voltage. The $I \sim V$ curves look like those of typical diodes, as shown in Fig. 1(a). The $I \sim V$ curves shifted along the horizontal axis as strain is applied, and the turn-on voltage increases from about 0.1 to 0.3 V as the strain changes from 2% (tensile) to -2% (compressive). In the case of MISTDs, the $I \sim V$ curves also look like those of typical diodes, and the shape of the curves seems to have a marked non-linear shape when the bias voltage is larger than the turn-on voltage, as shown in Fig. 1(b). The $I \sim V$ curves shift when strain is applied and the turn-on voltage changes from about 0.15 to 1.0 V as the strain changes from 2% (tensile) to -2% (compressive). Strain has a much great influence on the performance of the MISTDs compared to MSMSDs.

In order to study the effect of the MgO layer on the output of the diodes, the performance of the devices are compared. The current of the diodes at +1.0 V bias are chosen as a key index. Currents at a series of strains ranging from -2% (compressive) to +2% (tensile) are shown in Fig.1(c). When no strains are applied to the ZnO layers, the current of the MISTD is smaller than that of

MSMSD, since there is an extra MgO barrier layer in the MISTB. When strain is applied to the ZnO layer, the currents of both diodes increase with tensile strain and decrease with compressive strain. However, it is quite interesting to note that the response of the MISTD to strain is much greater than that of the MSMSD, as the slope for the MISTD is much larger than that of the MSMSD, as shown in Fig. 1(c). Moreover, the current of the MISTD is almost zero at -2% compressive strain and increases to a value much higher ($\sim 600 \text{ nA}$) than that of the MSMSD ($\sim 400 \text{ nA}$). It can be concluded from the above results than inserting an MgO layer can greatly enhance the electromechanical performance of ZnO based diodes, which is in agreement with our experimental results⁴⁰.

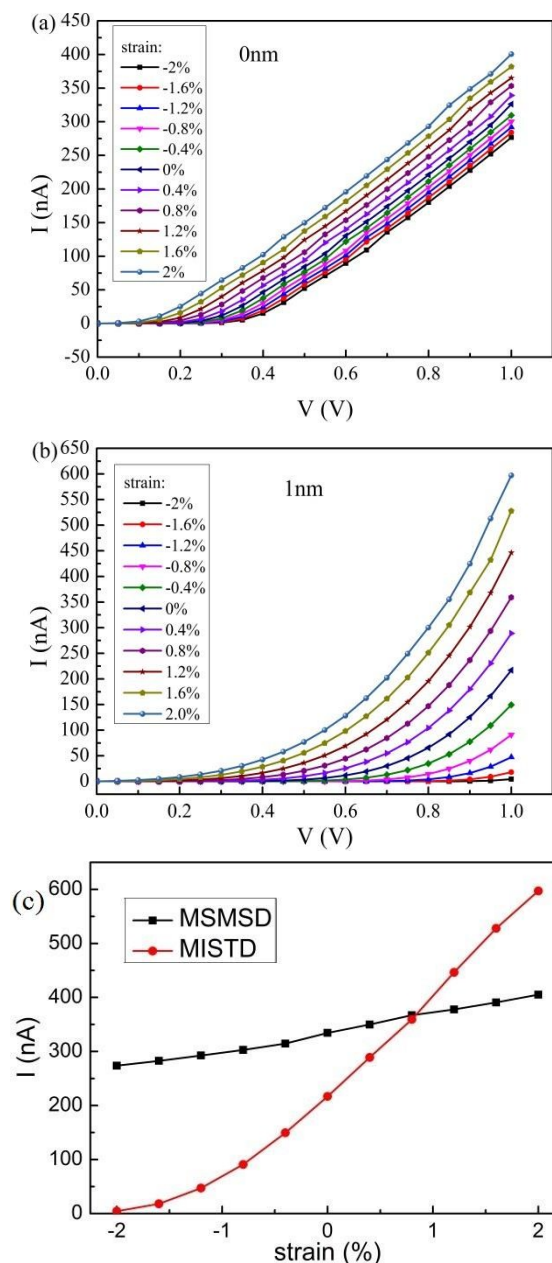


Figure 1 I-V characteristics under different strains of (a) a MSMSD and (b) a MISTD, (c) currents vs. strain plots of a MSMSD and a MISTD under +1.0 V bias.

2.2 Mechanism of the electromechanical effects

In order to reveal some insight on the mechanism of the electromechanical effect in the MSMs and MISTDs, detailed electronic structures are investigated, such as the distributions of electron density, electric field and conduction band edge.

In the case of MSMs, the situation is quite similar to a typical Schottky type diode, as shown in Fig. 2(a)-(c). There is a depletion region at the ZnO side of the ZnO/metal interfaces due to the presence of a Schottky contact as shown in Fig. 2(a). The positive charge density in the depletion region produces an electric field which changes almost linearly with position. Negative electrostatic potentials are produced and the conduction band edges change at the ZnO side of the ZnO/Metal interface. Schottky barriers are formed and the Schottky barrier heights are the change of conduction band edge across the interface.

When strain is applied to the devices, two effects take place: (1) the change of band edge due to strain, i.e. the deformation potential, which is taken account of by nextnano program (2) piezoelectric potential is produced due to the strain induced interface charges at the ZnO/metal interface. When compressive strain is applied, negative piezoelectric charges accumulate at the Oxygen terminated [0001] surface of ZnO, which is also the MgO/metal interface in our calculation model. In this case, the depletion region expands and the electric field increases, which leads to a large negative piezoelectric potential and high conduction band edge, as shown in Fig. 2(a)-(c). While tensile strain is applied, the trend is the opposite of the former. The Schottky barrier height can be evaluated from the Fig. 2(a) and plotted in Fig. 2(d). It can be seen that the Schottky barrier height changes from 0.45 eV (unstrained) to 0.556 eV (-2% strain) and 0.313 eV (+2% strain). The change of Schottky barrier height under compressive and tensile strain is asymmetrical and asymmetrical response of strain sensor based on single ZnO nanowires was observed in our previous work⁴³.

In the case of MISTDs, the situation is more complicated due to the insertion of an insulator MgO layer, as shown in Fig.3 (a)-(c). An extra insulator MgO layer with interface charges on both sides have to be considered. When strain is applied, there is also a depletion region at the ZnO side of the ZnO/MgO interfaces, and no net charges in the MgO layer, as shown in Fig. 3(a). Interface charges are accumulated on both side of the MgO layer. Electric fields are produced according to the electron distribution: a nearly linear electric field similar to that of a Schottky diode in the ZnO layer and constant one in the MgO layer with abrupt changes at the interface, as shown in Fig. 3(b). The conduction band edge is modulated by the induced electrostatic potential, and a two barrier model is found as we previously reported¹.

As ZnO is compressively strained, negative charges accumulate at the ZnO/MgO interface due to the piezoelectric effect, which leads to the expansion of the depletion region, as shown in Fig. 3(a). Due to the electron depletion region and interface charges at the ZnO/MgO interface, the almost linear and positive electric fields that appear in the ZnO layer are increased. Due to the lack of electrons in the insulating MgO layer and strain induced interface charges, the negative and constant electric field in the MgO layer increases, as shown in Fig. 3(b). The resulting electrostatic potential changes the

conduction band edge, and yields a wider and higher barrier (0.85V at -2% strain) in the ZnO layer and much higher barrier in the MgO layer, as shown in Fig. 3(c).

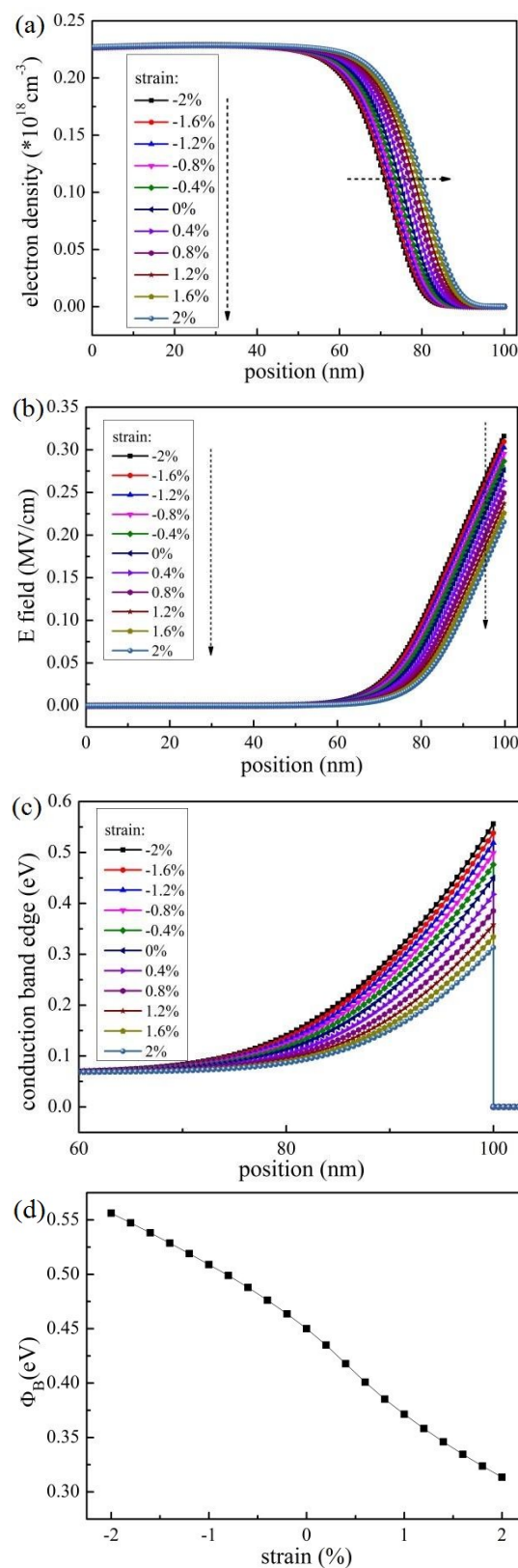


Figure 2. The distributions of (a) electron density (b) electric field, (c) conduction band edge of the MSMs and (d) Schottky barrier height under different strains without bias voltages.

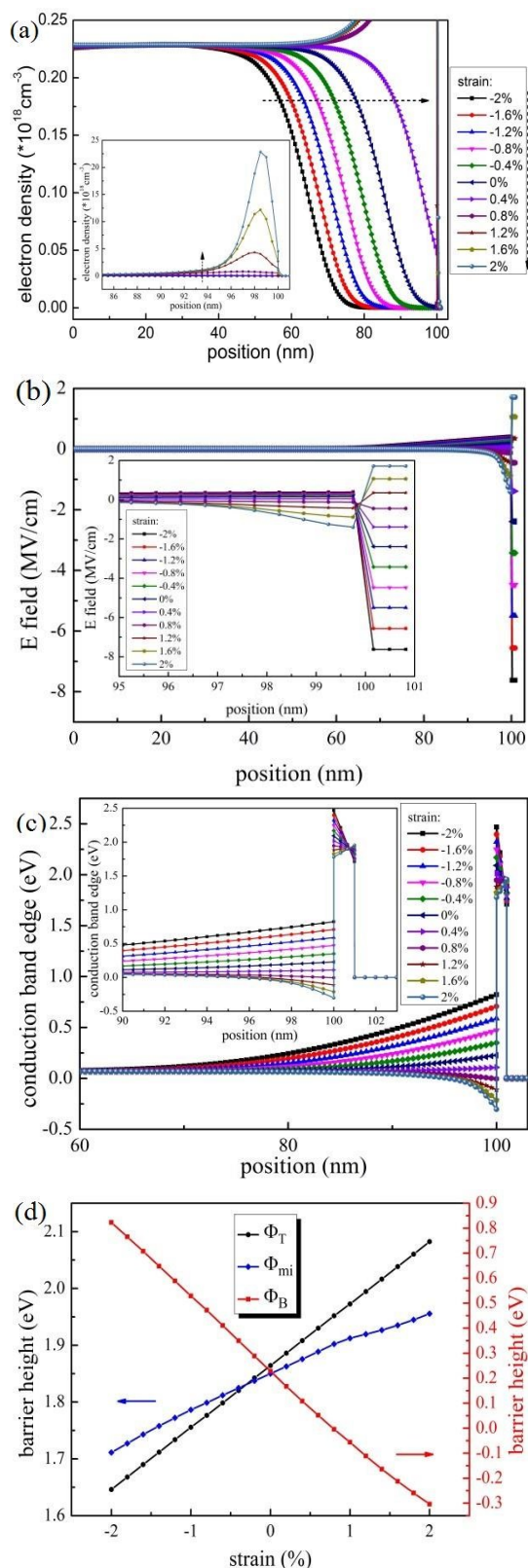


Figure 3 The distributions of (a) electron density, (b) electric field, (c) conduction band edge of the MISTD, and the insets show the detailed distribution near the ZnO-MgO-metal junctions. (d) The conduction band edge drop at ZnO/Mg interface Φ_T , barrier heights of MgO layer Φ_{mi} , barrier heights of ZnO layer Φ_B of the MISTD as functions of strain.

When tensile strain is applied, the situation changes in the opposite direction as compared to the case of compressive strain. The depletion region shrinks all the way until it disappears when the tensile strain is larger than 0.4%. At that point a large enough amount of electrons accumulates at the ZnO side of the ZnO/MgO interface and the direction of electric field flips, as shown in Fig 3(a)-(b). The energy barrier in the ZnO layer disappears while the energy barrier in the MgO layer is significantly reduced, as shown in Fig. 3(c).

The drop in the conduction band edge at ZnO/MgO interface (Φ_T), barrier heights of the MgO layer (Φ_{mi}), barrier heights of the ZnO layer (Φ_B) of the MISTD are evaluated and plotted in Fig. 3(d). The height Φ_B of the energy barrier between ZnO/MgO increases with compressive strain and decreases with tensile strain. The change rate is much faster in the case of MISTDs than that in the case of MSMDS. Meanwhile, Φ_T and Φ_{mi} change with strain due to piezoelectric effect and deformation potential. Both of them increase as the strain increased from -2% (compressive) strain to 2% (tensile).

Since the change of MgO layer thickness is neglected in our calculation, we can discuss on the deviation due to this effect. The insulating MgO layer leads to highly strain sensitive energy barrier in the ZnO layer and a high energy barrier in MgO layer with strain modulated height, as shown in Fig. 3(c). It can be seen clearly that the strain effect due to the barrier in ZnO layer is much larger than that due to the barrier in MgO layer, and the strain effect in the MgO layer due to the change in height ($\sim 10\%$) is much larger than that due to the change in layer thickness ($\sim 2\%$).

2.3 Enhancement mechanism of the MgO layer

With the above experimental results, the enhancement mechanism of the piezoelectric performance of MISTDs due to insertion of an MgO layer can be investigated. The above results show enhanced electromechanical performance. Two contributions need to be considered here: deformation potential and piezoelectric effect.

In the case of MSMDS, where the ZnO layer contacts directly with the metal electrode, strain induced dipoles are screened by external charges, and the adjustment function of the piezoelectric potential is inhibited. The piezoelectric response serves as a basis for comparison between MSMDS and MISTDs.

In the case of MISTDs, the change in the energy barrier heights of the MgO layer (Φ_{mi}), i.e. conduction band edge drop at the MgO/metal interface, is determined by the deformation potential. This changes from ~ 1.7 eV to 1.95 eV as the strain changes from -2% to 2%.

The MgO layer induces a very high energy barrier for electronic transport, and the strain induced interface charges at the ZnO/MgO interface take the value that is expected if the piezoelectric charges are not screened. Screen charge is accumulated at the MgO/metal interface and an effective capacitor is formed. The strain induced interface charge q_s can be expressed in terms of the effective piezoelectric coefficients as follow:

$$q_s = LS e_{33}^{eff} \epsilon_3 \quad (1)$$

where L and S are the length and cross section area of the ZnO nanowire, e_{33}^{eff} is the effective piezoelectric coefficient, in the [0001] direction coupling with strain ϵ_3 in the same direction, of the ZnO nanowires.

The electrostatic field is adjusted by both strain induced interface charge and the conduction band edge change $\Delta\phi_{pz}$ at the left side of MgO layer with respect to the right side is:

$$\Delta\phi_{pz} = -\frac{1}{4\pi\epsilon} q_s d / S \quad (2)$$

where ϵ is the dielectric constant of MgO and d is the MgO layer thickness. Hence, $\Delta\phi_{pz}$ can be written as:

$$\Delta\phi_{pz} = -\frac{1}{4\pi\epsilon} L d e_{33}^{eff} \epsilon_3 \quad (3)$$

It can be seen that the conduction band edge change across the MgO layer is proportional to the strain and layer thickness. The conduction band edge at the left side of MgO layer is determined by two factors: deformation potential of the MgO layer and the electrostatic potential change across the MgO layer. It is found that the conduction band edge decreases sharply from about 2.5 eV to 1.8 eV as the strain changes from -2% to 2%.

The barrier height Φ_B in the ZnO layer is determined by the conduction band edge at the left side of MgO layer minus the conduction band edge drop at the ZnO/MgO interface (Φ_T), which is mainly determined by the deformation potential of ZnO and MgO. The barrier height Φ_B decreases from 0.85eV to -0.3 eV, and the rate of change with strain is much larger than that of the MSMSD.

By comparing the change of conduction band edges with strain between the MSMSDs and MISTDs, it is quite apparent that strain has a much larger effect on the former, since the barrier height and width in the ZnO layer vary at a much higher rate compared to that of the MSMSDs. Furthermore the barrier height of the MgO layer also varies by a considerable amount under strain. This is due to the fact that the strain induced charges are accumulated at the left side of the insulating MgO layer and screening charges appear on the right hand side. The induced electrostatic potential modulate both the height of the energy barrier in the MgO layer, but also the height and width of the energy barrier in the ZnO layer. In the case of MSMSDs, strain induced charges are screened by external charges and produce an energy barrier in the ZnO layer which changes slowly with strain. Therefore, the origin of the enhanced electromechanical performance of MISTDs is due to the inhibition of screening effect induced by the insulating MgO layer, which leads to a highly strain sensitive modulated energy barrier

Conclusions

In summary, the electromechanical performances of MISTDs based on Metal-MgO-ZnO nanostructures were investigated and it is found that the performance of ZnO based diodes is greatly improved by inserting a MgO layer. The piezoelectric response of MISTDs and the change of Schottky barrier height with strain is much higher than that of MSMSDs. The current of the MISTD is almost zero at -2% compressive strain and increases to a much higher value (~ 600nA) as compare to that of the MSMSDs (~ 400 nA) at +2% tensile strain. Detailed electronic structure investigation found that the origin of the enhanced electromechanical performance of MISTDs is due to the inhibition of screening effect by the insulating MgO layer which leads to a highly strain sensitive energy barrier in the ZnO layer and an extra MgO layer with strain modulated energy barrier height.

Computational details

As a convenient choice for calculation, we build a 1D nanostructure model as shown in Fig. 4, using a similar approach as used in our previous report¹. The ZnO and MgO layer thicknesses are 100nm and 1 ~ 2 nm respectively, and the axial direction is along the [0001] crystal orientation. The n-type doping concentration in the ZnO is $5 \times 10^{17} \text{ cm}^{-3}$. The left contact of the MISTD is set to ohmic, while the right contact is set as a Schottky type. In our calculation, the layer thickness is fixed and it will not change due to applied strains which will leads to some deviations.

The Schottky barrier height between ZnO and the metal is set to 0.45 eV while the barrier height between MgO and the metal is set to 1.85eV. The effective height of the tunneling barrier between ZnO/MgO is taken as $\Phi_T = 1.7\text{eV}$, equal to the band offset between ZnO/MgO. The piezoelectric constants of ZnO are as follow: $e_{33}=1.34 \text{ C/m}^2$, $e_{31}= -0.57 \text{ C/m}^2$. The other material parameters used in the calculations are given in Table 1.

To simplify the calculation, the effective mass approximation (EMA) was used for the conduction band electrons in both ZnO and the MgO layers. The predictor-corrector-type method was adopted for the Schrödinger and Poisson equations and an under-relaxation approach was used for the current equations, as detailed in our previous report¹.

As a thin MgO layer is deposited on a thick ZnO layer, the ZnO layer is set to be unstrained. The lattice mismatch between the ZnO and MgO results in biaxial strain in the MgO layer as follow:

$$\epsilon_{xx} = \epsilon_{yy} = \frac{a_{\text{ZnO}} - a_{\text{MgO}}}{a_{\text{MgO}}} \quad (4)$$

$$\epsilon_{zz} = -2 \cdot \frac{C_{13}}{C_{33}} \cdot \epsilon_{xx} \quad (5)$$

where C_{13} and C_{33} are the elastic constants of MgO. The z (x, y) axis is taken to be parallel (perpendicular) to the [0001] crystal direction. The initial strains of MgO are $\epsilon_{xx} = \epsilon_{yy} = -1.19\%$ and $\epsilon_{zz} = -1.13\%$, respectively. When the strain is applied to the ZnO layer, the strain of the MgO layer changes accordingly.

Table I Parameters of ZnO and MgO used in the simulation

parameter		ZnO	MgO
lattice constant (nm) ⁴⁴	a	0.325	0.3289
	c	0.521	0.5031
band gap (eV) ⁴⁵	E _v	3.4	6.3
	$m_{e\perp}^*$	0.24 ⁴⁶	0.35 ⁴⁷
	$m_{e\parallel}^*$	0.28 ⁴⁶	0.35 ⁴⁷
	$m_{h\perp}^*$	0.54 ⁴⁶	2.77 ⁴⁷
effective mass	$m_{h\parallel}^*$	2.74 ⁴⁶	1.6 ⁴⁷
	ϵ_s	8.91 ⁴⁸	9.83 ⁴⁹
static dielectric constants			
electron mobility (cm ² /Vs)	μ_n	205 ⁵⁰	2 ⁵¹
	C ₁₁	206	222
elastic constants (GPa) ⁵²	C ₁₂	118	90
	C ₁₃	118	58
	C ₃₃	211	109
	C ₄₄	44	105
deformation potential (eV) ⁵³	a _{c,c}	-3.06	-1.95
	a _{c,a}	-2.46	-7.96

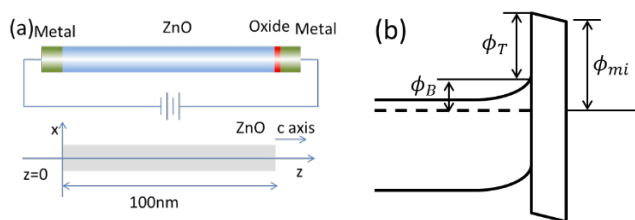


Figure 4 A 1D nanostructure model of the Metal-MgO-ZnO MISTD used in the simulation. (a) a schematic diagram of the model (b) band structure diagram

Acknowledgements

This work was supported by the National Basic Research Program of China (No. 2013CB932602), the Program of Introducing Talents of Discipline to Universities (No. B14003), National Natural Science Foundation of China (Nos. 51572021, and 51527802), Beijing Municipal Science & Technology Commission, and the Fundamental Research Funds for Central Universities, the Newton International Research Collaboration Programme (No. NRCP/1415/129).

References

- X. Yang, Y. Gu, M. A. Migliorato and Y. Zhang, *Nano Research*, **2016**, DOI 10.1007/s12274-016-1024-y.
- K-W. Chung, Z. Wang, J. C. Costa, F. Williamson, P. P. Ruden and M. I. Nathan, *Appl. Phys. Lett.*, 1991, **59**, 1191.
- Z. L. Wang, J Song, *Science*, 2006, **312**, 5771.
- T. Zimmermann, M. Neuburger, P. Benkart, F. J. Hernandez-Guillen, C. Pietzka, M. Kunze, I. Daumiller, A. Dadgr, A. Krost, E. Kohn, *IEEE Elec. Device Lett*, 2006, **27**, 309.
- C. H. Wang, W. S. Liao, Z. H. Lin, N. J. Ku, Y. C. Li, Y. C. Chen, Z. L. Wang, *Adv. Energy Mater.*, 2014, **4**, 1400392
- Z. Zhang, Q. L. Liao, X. Q. Yan, Z. L. Wang, W. D. Wang, X. Sun, P. Lin, Y. H. Huang, Y. Zhang, *Nano Research*, 2014, **7**, 190.
- H. Y. S. Al-Zahrani, J. Pal, M. A. Migliorato, *Nano Energy*, 2013, **2**, 1214.
- X. B. Han, L. Z. Kou, X. L. Lang, J. B. Xia, N. Wang, R. Qin, J. Lu, J. Xu, Z. M. Liao, X. Z. Zhang, X. D. Shan, J. Y. Gao, W. L. Guo, D. P. Yu, *Adv. Mater*, 2009, **21**, 4937.
- X. Xiao, L. Y. Yuan, J. W. Zhong, T. P. Ding, Y. Liu, Z. X. Cai, Y. G. Rong, H. W. Han, J. Zhou, and Z. L. Wang, *Adv. Mater.*, 2011, **23**, 5440.
- W. Han, Y. Zhou, Y. Zhang, Y. Zhang, C. Y. Cheng, L. Lin, X. Wang, S. H. Wang, and Z. L. Wang, *ACS Nano*, 2012, **6**, 3760.
- Q. L. Liao, Z. Zhang, X. H. Zhang, M. Mohr, Y. Zhang, *Nano Research*, 2014, **7**, 917.
- S. N. Lu, Q. L. Liao, J. J. Qi, S. Liu, Y. C. Liu, Q. J. Liang, G. J. Zhang, Y. Zhang, *Nano Research*, 2016, **9**, 372.
- Y. Yang, J. J. Qi, W. Guo, Y. S. Gu, Y. H. Huang and Y. Zhang, *Phys. Chem. Chem. Phys.*, 2010, **12**, 12415.
- Q. L. Liao, M. Y. Liang, Z. Zhang, G. J. Zhang, and Y. Zhang, *Nano Research*, 2015, **8**, 3772.
- C. F. Pan, S. Niu, Y. Ding, L. Dong, R. M. Yu, Y. Liu, G. Zhu, and Z. L. Wang, *Nano Lett.*, 2012, **12**, 3302-3307.
- G. Romano, G. Mantini, A. D. Carlo, A. D. Amicoet, C. Falconi and Z. L. Wang, *Nanotechnology*, 2011, **22**, 465401.
- Y. Hu, Y. Zhang, C. Xu, L. Lin, R. L. Snyder, and Z. L. Wang, *Nano Letters*, 2011, **11**, 2572-2577.
- Z. Z. Shao, L. Y. Wen, D. M. Wu, X. A. Zhang, S. L. Chang, and S. Q. Qing, *J. Appl. Phys.*, 2010, **108**, 124312.
- J. I. Sohn, S. N. Cha, B. G. Song, S. Lee, S. M. Kim, J. Ku, H. J. Kim, Y. J. Park, B. L. Choi, Z. L. Wang, J. M. Kim, and K. Kim, *Energy Environ. Sci.*, 2013, **47**, 97-104.
- Z. Zhang, Q. L. Liao, Y. H. Yu, X. D. Wang, Y. Zhang, *Nano Energy*, 2014, **9**, 237-244.
- Y. F. Hu, L. Lin, Y. Zhang, Z. L. Wang, *Adv. Mater.*, 2012, **24**, 110-114.
- K. Y. Lee, J. Bae, S. Kim, J. Lee, G. C. Yoon, M. K. Gupta, S. Kim, H. Kim, J. Park, S. Kim, *Nano Energy*, 2014, **8**, 165-173.
- A. Wei, L. Pan, W. Huang, *Mater. Sci. Eng.: B*, 2011, **176**, 1409-1421.
- Z. L. Wang, *MRS Bulletin*, 2012, **37**, 814-827.
- Z. L. Wang, *Adv. Mater.*, 2012, **24**, 4632.
- W. G. Zhang, R. Zhu, V. Nguyen, R. Yang, *Sensor. Actuat. A: Phys.* 2014, **205**, 164.
- Q. L. Liao, M. Mohr, X. H. Zhang, Z. Zhang, Y. Zhang, H. J. Fecht, *Nanoscale* 2013, **5**, 12350.
- S. N. Lu, J. J. Qi, Z. Z. Wang, P. Lin, S. Liu, Y. Zhang, *RSC Adv.* 2013, **3**, 19375.
- X. Q. Liao, X. Q. Yan, P. Lin, S. N. Lu, Y. Tian, Y. Zhang, *ACS Appl. Mater. Interfaces.* 2015, **7**, 1602.
- Q. L. Liao, Z. Zhang, X. H. Zhang, M. Mohr, Y. Zhang, H. J. Fecht, *Nano Research*, 2014, **7**, 917.
- X. N. Wen, W. Z. Wu, Y. Ding, Z. L. Wang, *Adv. Mater.* 2013, **25**, 3371.
- S. J. Young, L. W. Ji, S. J. Chang, S. H. Liang, K. T. Lam, T. H. Fang, K. J. Chen, X. L. Du, Q. K. Xue, *Sensor. Actuat. A: Phys.* 2008, **141**, 225.
- M. Afsal, C. Y. Wang, L. W. Chu, H. Ouyang, L. J. Chen, J. Mater. Chem. 2012, **22**, 8420.
- Y. Liu, S. M. Niu, Q. Yang, B. D. B. Klein, Y. S. Zhou, Z. L. Wang, *Adv. Mater.* 2014, **26**, 7209.
- C. Y. Liu, H. Y. Xu, J. G. Ma, X. H. Li, X. T. Zhang, Y. C. Liu, R. Mu, *Appl. Phys. Lett.* 2011, **99**, 063115.
- H. Zhu, C. X. Shan, J. Y. Zhang, Z. Z. Zhang, B. H. Li, D. X. Zhao, B. Yao, D. Z. Shen, X. W. Fan, Z. K. Tang, X. H. Hou, C. Kwang-Leong, *Adv. Mater.* 2010, **22**, 1877.
- S. N. Lu, J. J. Qi, Y. S. Gu, S. Liu, Y. Zhang, *Nanoscale*, 2015, **7**, 4461.
- C. Q. Qin, Y. S. Gu, X. Q. Wang, X. Sun, Y. Zhang, *Nano Research*, 2015, **8**, 2073.
- Q. L. Liao, M. Y. Liang, Z. Zhang, G. J. Zhang, Y. Zhang. *Nano Research*, 2015, **8**, 3772.
- X. Q. Liao, X. Q. Yan, P. Lin, S. N. Lu, Y. Tian, Y. Zhang. *ACS Appl. Mater. Interfaces.* 2015, **7**, 1602.
- S. Birner, T. Zibold, T. Andlauer, T. Kubis, M. Sabathil, A. Trellakis, P. Vogl, *IEEE T. Electron Dev.* 2007, **54**, 2137.
- Y. Zhang, Y. Liu, Z. L. Wang, *Adv. Mater.*, 2011, **23**, 3004.
- P. Wang, Y. Gu, P. Lin, Y. Zhao, Y. Hu, Y. Min, Y. Zhang, *J. Nanoscience and Nanotechnology*, 2014, **14**, 6084.
- K. Shimada, N. Takahashi, Y. Nakagawa, T. Hiramatsu, and H. Kato, *Phys. Rev. B*, 2013, **88**, 75203.
- A. Janotti, C. G. Van de Walle, *Phys. Rev. B*, 2007, **75**, 121201.
- W. R. L. Lambrecht, A. V. Rodina, S. Limpijumngong, B. Segall, and B. K. Meyer, *Phys. Rev. B*, 2002, **65**, 75207.
- Y. Xu, W. Y. Ching, *Phys. Rev. B*, 1991, **43**(5), 4461-4472.
- N. Ashkenov, B. N. Mbenkum, C. Bundesmann, V. Riede, M. Lorenz, D. Spemann1, E. M. Kaidashev, A. Kasic, M. Schubert, M. Grundmann1, G. Wagner, H. Neumann, V. Darakchieva, H. Arwin, and B. Monemar, *J. Appl. Phys.*, 2003, **93**, 126.
- M. Wintersgill, J. Fontanella, C. Andeen, and D. Schuele, *J. Appl. Phys.*, 1979, **50**, 8259.

- 50 D. C. Look, D. C. Reynolds, J. R. Sizelove, R. L. Jones, C. W. Litton, G. Cantwell, W. C. Harsch, *Solid State Commun.*, 1998, **105**, 399-401.
- 51 E. Yamaka, K. Sawamoto, *Phys. Rev.*, 1956, **101**, 565.
- 52 P. Gopal, N. A. Spaldin, *J. Elec. Mater.*, 2006, **35**, 538.
- 53 Q. Yan, P. Rinke, M. Winkelkemper, A. Qteish, *Appl. Phys. Lett.*, 2012, **101**, 152105